AN ANALYSIS OF HARDNESS OF LASER WELDS

Final report on a
Government of Canada, Department of Supply and Services
Contract for the
Department of Energy Mines and Resources.

Contract Serial Number OSQ85-00155
D.S.S. File Number OSSQ.23440-5-9187

Contractor:

V.E. Merchant
ELECTRICAL AND OPTICAL RESEARCH
4211 35th Avenue, Leduc, Alberta, Canada, T9E 3C8.
403-986-6158

Scientific Authority:

Dr. J.T.M. McGrath,
Dept. of Energy Mines and Resources,
CANMET - Phys. Met. Res. Labs (PMRL)
555 Booth Street,
Ottawa, Ontario,
K1A 0G1

Science Procurement Officer:

Ms. Gaetane Dagenais,
Department of Supply and Services,
Science and Professional Services Directorate,
Place du Portage, Phase III, 11C1,
11 Laurier Street,
Hull, Quebec,
K1A 0S5

4 of pp

MAR 3 1986
MICROMEDIA

Table of Contents

	Page
A. Executive Summary (English)	3
B. Executive Summary (French)	4
C. Introduction	5
D. Laser welding	7
E. The laser and laser welding equipment	12
F. Weld hardness measurements	14
G. Fusion zone measurements	18
H. Prediction of hardness of laser welds and HAZs	19
I. Comments on prediction of weld cooling rates	22
J. Special features of deep penetration welding	42

A. Executive Summary (English)

Laser welds have been performed using a new style of CO2 laser with a reliable high-quality output beam. The weld hardness was analyzed as a function of energy input to the weld and position through the weld cross-section. The hardness on the weld centerline corresponds to that which would be predicted on the basis of simple theoretical models or on a correlation of cooling rates with welding conditions in a variety of welding techniques. However, it appears that considerations involving the latent heat of fusion are more important in deep penetration processes such as laser welding than in other welding techniques, because of the low heat inputs involved. This remains to be confirmed by detailed finite element analysis and by experimental measurements of the cooling rate in the weld pool following laser welding.

The standard techniques used to predict the heat affected zone hardness can also be used in the case of autogenous laser welding to predict the fusion zone hardness. However the heat affected zone hardness was less than the predicted values because the high speed of the laser welding resulted in too short a diffusion time for the formation of homogeneous austenite. The formation of a homogeneous austenite is a prerequisite for the prediction of the hardness by established procedures. In predicting the hardness of the fusion zone in deep penetration welding processes, the time-at-temperature available for diffusion of carbon is at least as important as the cooling rate itself.

B. Executive Summary (French)

Résumé Exécutif:

Laser welds ont été utilisés au nouveau svtle de CO_2 laser avec un rendement sûr en rayons de haute-qualité. La solidité de la soudure fut analysée comme fonction d'énergie interieur à la soudure et sa position au travers la section croissée de la soudure. La solidité sur la ligne centrale de la soudure correspond à celle qui serait prédie basé sur les simples models théoriques ou sur une corrélation de taux de froideur avec conditions de soudure dans une variété de techniques. Néanmoins il semble que les considérations impliquant la chaleur latent de fusion sont plus inportant dans le procédé en pénétration profonde tel que le laser welding que dans les autres techniques de soudure à cause de la faible chaleur (inputs) impliqué. Ceci reste à être confirmé par l' analyse détailé d' élemént finite et par les measures expérimentales au taux de froideur dans le pool de soudure suivant laser welding.

Les techniques standard utilisées pour prédire la chaleur affectée de la zone solide peut aussi être utilisé dans le cas de soudure laser autogènes à prédire la fusion de zone solide. Cependant la chaleur affectée de la zone solide était moins que les valeurs predites à cause de la haute vitesse du laser welding resulta dans un temps de diffusion trop court pour la formation d' austenite homogène est unénecessité préalable pour la prédiction de la solidité par les procédures établies. En prédisant la solidité de la zone de fusion au procédé de soudure en pénétration profonde. La température à temps disponible pour diffusion de carbone est au moins aussi important que le taux de froideur lui-même.

C. Introduction

Since the discovery of lasers 25 years ago, they have developed from laboratory instruments to reliable industrial tools. Lasers are now used in production line environments in a variety of industries around the world. They have proved themselves to be a cost effective method of performing routine metal working tasks.

A new style of high power laser, unique for its reliability and quality of its output, has been recently developed. The laser was used to investigate the welding of HSLA steels. The hardness of the resulting welds, and a comparison between the measured values and theoretical predictions, is presented.

For each type and thickness of steel, a weldability lobe exists. This weldability lobe consists of the set of points of laser power and welding speed at which cosmetically pleasing welds with complete penetration can be prepared. In a laser welding programme at Majestic Laser Systems, a weldability lobe for one type of HSLA steel had been partially determined. The maximum speed at which cosmetically pleasing welds could be made was not determined due to the limitations in the workpiece handling equipment. Therefore the weldability lobe was not closed at the upper end. Previous researchers have reached similar limitations and it is not known whether in fact the weldability lobes are open ended or whether maximum welding speeds and corresponding power levels do exist.

Welds at several points on the lobe were tested for hardness. The results show that the metallurgical qualities of welds may vary through out the weldability lobe. Tensile or bending tests on these welds have not been performed, and hardness itself cannot be used to establish criteria for acceptable welding techniques. However a variation of hardness throughout the weldability lobe is a good indication that other properties such as the tendancy towards brittle fracture may also vary. A weldability lobe defined by "acceptable metallurgical characteristics" may be smaller that that defined by "acceptable cosmetic appearance".

Shing, Bibby, and Goldak of Carleton University have recently summarized methods of calculating weld hardness on the basis of welding parameters. They apply these methods to calculating the hardness of the Heat Affected Zone. However in autogenous laser welding the chemistry of the weld metal is well established, and the methods of calculation summarized by Shing *et al.* should be applicable to the weld metal of laser welds in addition to the HAZ. Their calculation proceeds in two halves, first calculating the cooling time on the basis of the welding parameters and secondly evaluating the hardness from the cooling time and the steel composition.

The present work involves an analysis of the hardness of laser welds. Various methods of calculating the cooling rate of the weld and heat-affected-zone metal are analyzed. The predictions by various models of the cooling time and resulting hardness on the weld centerline as a function of welding energy input are compared.

From a weld cross-section the amount of energy required to provide the latent heat of fusion for the weld metal can be calculated. This was done for the welds whose hardness is analyzed here and for a comparison of laser welding with other welding processes. The latent heat of fusion is released late in the thermal cycle and distorts the spatial and temporal temperature dependence. A simple one dimensional numerical integration of the heat flow equations is performed. The resulting thermal cycles are compared in cases where realistic values of the latent heat are considered and when the latent heats are ignored.

The report concludes with an analysis of special features of laser welding, or more generally of deep penetration welding processes. These special features must be considered when applying thermal cycle models that are successful in analyzing conventional welding processes.

Because of the high speed, the cost per inch of weld by lasers is comparable to or less than that by more conventional welding processes. As industrial procedures become more mechanized, lasers will be playing an ever-increasing role, and it is important to understand the detailed mechanisms of laser-material interactions.

D. Laser welding

When a high power laser beam is focussed onto a metal surface, the metal is initially highly reflective for the infrared energy. But a small fraction of the energy is absorbed, and this heats the metal. As the metal gets hot, the reflectivity decreases and a larger fraction of the energy is absorbed. Thus if a beam is intense enough to overcome the initially small absorption of energy, a significant fraction of the beam will be absorbed. At the point of contact between an intense focussed beam and a metal surface, the metal heats to the point that it vaporizes. This creates a hole in the material, called a keyhole. The keyhole is filled with metal vapor, and the pressure of the metal vapor keeps the hole open.

As the beam scans over the metal surface, the keyhole moves through the material. The metal at the front of the keyhole is continuously being melted, and some of it vaporized, while the molten material at the rear of the keyhole is resolidifying. The hole is completely surrounded by a layer of molten material, in which metal flows from the front of the hole to the rear, where it solidifies again. Some of the metal crosses the hole in the form of vapour, but this does not seem to be the main method of transfer. The fluid flow occurs as a result of viscosity gradients due to the difference in temperature between the leading and trailing edges of the keyhole, and can be turbulent.

The effect of the laser beam is to melt the material at the point of contact between the beam and the surface, and allow it to resolidify behind the beam. If there is a butt joint, the material in both pieces of metal is melted, but they resolidify to form a single piece of material - a fusion join without the addition of filler material.

This process is called keyhole or deep penetration welding. The depth of the fusion zone can be five or as much as ten times the width of the melt. Figure 1 shows the upper bead and the cross-section of a laser beam weld in 3/8 inch thick HSLA steel.

The scalability of high power laser welding is illustrated in figure 2, for a 1/2 inch thick steel. This figure is from an experimental program conducted at the Welding Institute in the U.K. (Watson, 1984). A similar curve could be derived for other steels and other thicknesses. It can be seen that for a given power level, if the metal is moved too fast, insufficient penetration results. However if the metal moves too slowly, the molten material simply falls out of the keyhole before it has a chance to resolidify. This results in a cutting action which can be greatly enhanced by the use of a reactive gas jet. For intermediate values of the scanning speed, welds without porosity and with a cosmetically pleasing external appearance can be readily

obtained.

The diagonal lines of figure 2 indicate the locus of constant energy input. It is readily seen that within the lobe of acceptable welds the energy input varies from 450 to 720 Joules per millimeter of weld. The work described in this report and in the earlier work at The Welding Institute indicates that the weld centerline hardness increases as the energy required to do the weld decreases. This variation of properties would mean that the weldability lobe as shown in figure 2 might be considerable smaller if defined in terms of "acceptable metallurgical characteristics" instead of in terms of "acceptable cosmetic appearance". In particular the weldability lobe shown in the figure is open at the high power region due to the power limitations of the laser used to do the welding. When metallurgical characteristics are considered, the weldability lobe may not be open at the high speed high power end. In other words, there may be a maximum welding speed that would result in welds of sufficient toughness.

The weldability lobe for different material thicknesses of A36 steel is shown in figure 3. As the thickness is increased, the tolerance in welding speed or laser power becomes increasingly thinner. These results are from measurements at the Naval Research Laboratory in the United States (Metzbower *et al.*, 1983).

References for Section D.

Metzbower, E.A., Hella, R.A., and Theodorski, G., 1983. *"Laser Beam Welding at Nirop, A Navy Manufacturing Technology Program"*, in Lasers in Material Processing, Ed. by E.A. Metzbower, pg 266-272 (American Society for Metals, Metals Park, Ohio).

Watson, M.N., 1985. *"Laser Welding of a 12.5 mm thick niobium microalloyed structural steel at powers of up to 9kW"*, presented at the Second International Beam Technology Conference, Essen, W.Germany.

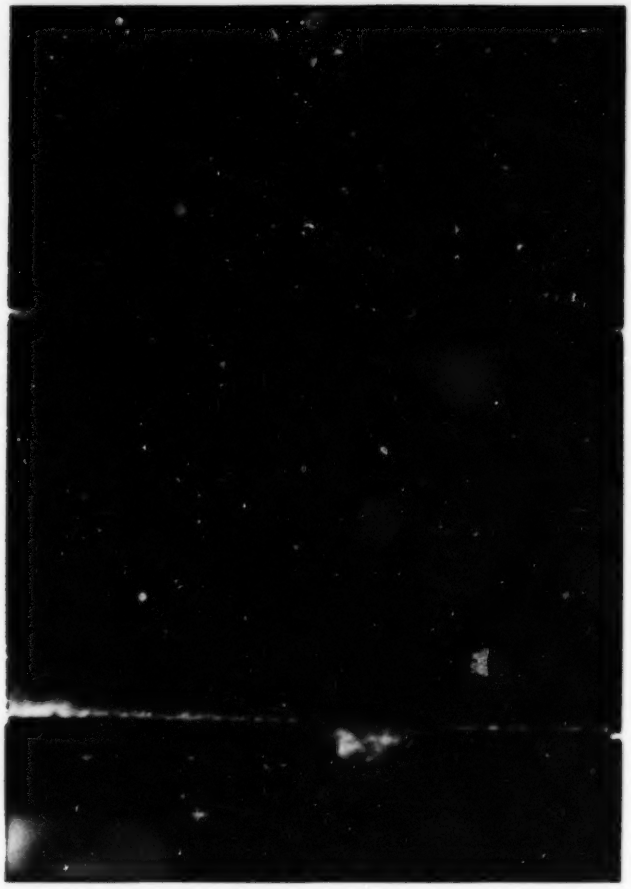

Figure 1.

Cross-section and Upper Bead of Laser Weld
in 9.5 mm thick HSLA Steel

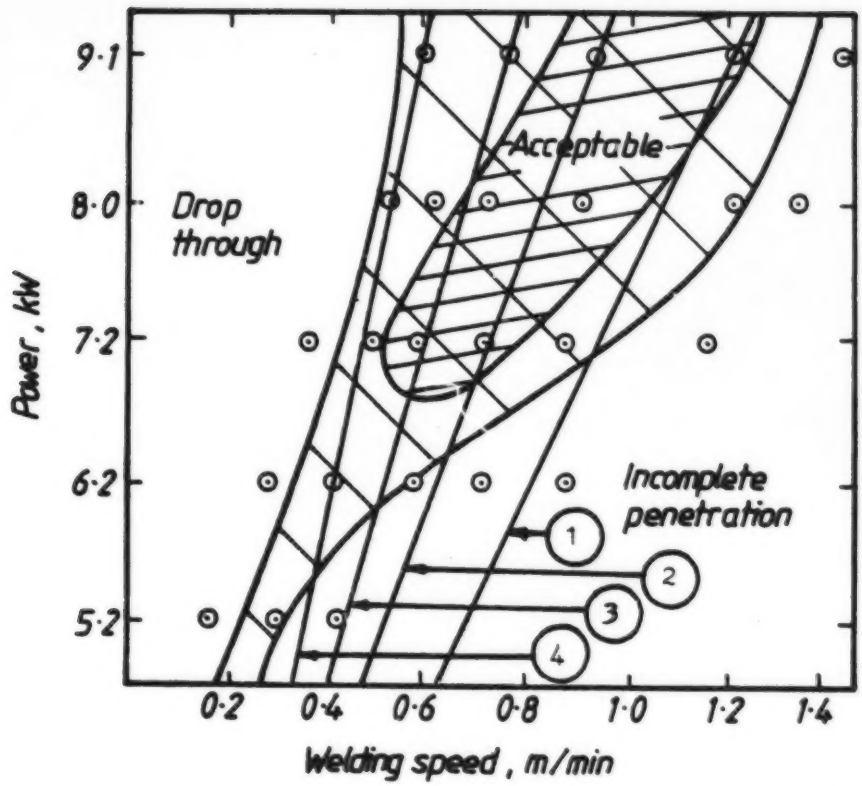

Figure 2. Conditions for cosmetically pleasing porosity-free laser welds in fully killed steel of 12.5 mm thickness. The diagonal lines indicate constant energy input, as follows: 1-4.55 kJ/cm; 2-5.9 kJ/cm; 3-7.2 kJ/cm; 4-8.95 kJ/cm. From Watson (1985)

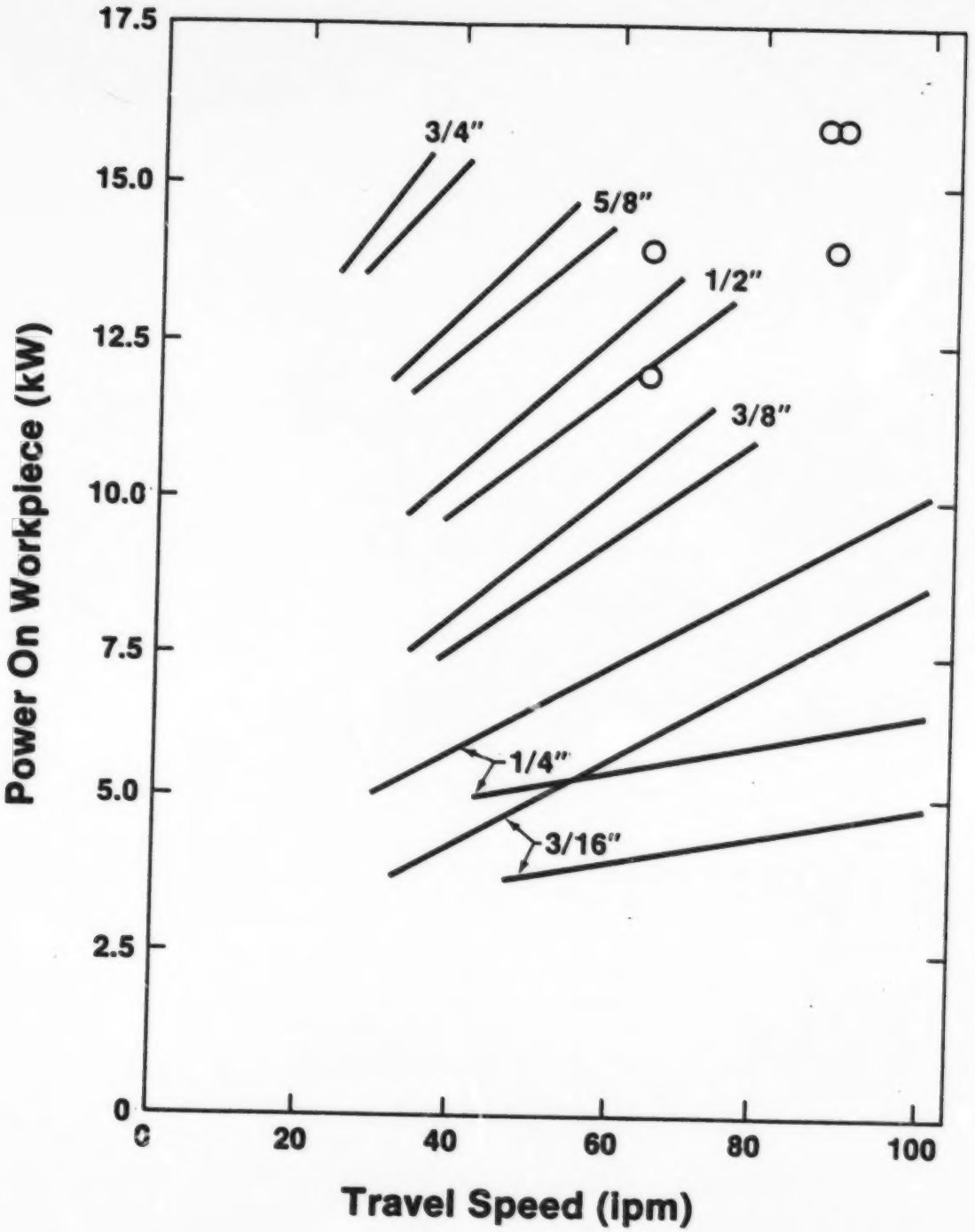

Figure 3. Laser welding conditions for different material thicknesses. The circles indicate the conditions used for the welds studied in this report.

E. THE LASER AND LASER WELDING EQUIPMENT

The CO2 laser and laser welding equipment used for this work have been described in detail elsewhere (Merchant, 1985; Majestic Laser Systems, 1984).

Neither the internal pipe clamp or the seam tracker described in the above referenced report were used in the work described here which involved bead-on-plate welds (or, more correctly, bead-on-pipe welds.) Only those welds in which full penetration of the workpiece and cosmetically pleasing upper and lower beads were achieved were analyzed for hardness.

A commercially available pipe roller was used. However it was found that the speed of rotation of the pipe roller fluctuated and was not accurately resettable. The motor driving the rollers was replaced by a more precise motor and gear reduction unit that could control the speed to about 2% accuracy.

The focussing head with a 70 cm. focussing mirror produces a focussed beam size of 0.4 mm. at the 2 kilowatt power level, increasing to 1.2 mm. at 20 kW. These figures are for the full width at half maximum of the intensity distribution.

A gas shielding nozzle (not described in the above referenced report) was used for plasma suppression and to protect the molton material from the atmosphere. The plasma suppression jet directed 17 standard liters per minute of helium at 45 degrees onto the point of contact between the beam and the surface. The trailing gas shield used helium at 13 SLPM. The gas nozzle used here was patterned after one used at Culham laboratories and was not considered optimum for either a research or production environment.

A sliding mirror could be inserted into the beam path between the laser and the focussing head which focussed the beam on the workpiece. The sliding mirror deflected the beam into a rotating cone calorimeter (Seguin, Sequin, Dow, and Nath, 1984). A power reading was obtained before each weld was performed. The measured power in kilowatts was divided by the pipe rolling speed in cm/sec to obtain the heat input for welding.

References in Section E.

Majestic Laser Systems, July 1984. "The preparation and evaluation of welds made in pipeline steels by the laser welding process", Mid-Term Report on Government of Canada Department of Supply and Services Contract OSQ83-00264.

Merchant, V.E., 1985. "Development of a New 20-kW CO2 Laser", Laser Focus and Electro-Optics Magazine, Vol. 21, p 162-166.

Seguin, H.J.J., Seguin, V.A., Dow, J., and Nath, A.K., 1984. "A new calorimeter for intense laser radiation", Appl. Phys. B33, 239-241 (1984).

F. Weld Hardness Measurements

The experimental results reported here involved a series of measurments of welding speed versus laser powers on 3/8 inch (9.5 mm) HSLA steel. The composition of the steel is given in table 1. Full penetration bead-on-plate welds were performed with powers ranging from 12 to 16 kilowatts on the pipe, and at speed ranging up to 3.8 cm/sec. Points indicating the welding conditions under which the welds analyzed here were obtained are indicated on figure 3. This figure also indicates the operating conditions needed to perform welds in various thicknesses of A36 plate, from work done at the NRL. Note that the for the same thickness of steel and the same welding speed, the results presented here required approximately 20% more laser power. The reason for this is not known.

Table 1. Steel Composition

C	0.07%	Mn	1.54%	P	0.008%	S	0.014%
Si	0.11%	Cu	0.13%	Ni	0.06%	Cr	0.03%
Mo	0.024%	V	0.071%	Cb	0.034%	Al	0.012%
Sn	0.008%	Fe	Balance				

The microhardness of each of the welds obtained under the conditions indicated on figure 3 was obtained using the Vicker's diamond pyramid method at various positions through the fusion, heat affected zone and base metal, near the top surface and near the bottom surface of the weld. The results are presented in figure 4 for several of the welds. Also shown in figure 4 are the microhardness that would be predicted on the basis of a simple cooling model, as will be discussed later. The hardness on the weld centerline near the upper bead is plotted as a function of the heat input to the weld in figure 5. The heat input is expressed as the power of the laser **q** divided by the linear velocity **v** of the workpiece under the focussing head. It can be seen that the weld center hardness decreases as the specific energy input used for welding increases.

For the welds that were analyzed here, the welding conditions and characteristics of the welds are summarized in Table 2. For each weld there were two measurements of the hardness in the weld metal approximately 1 mm. into the material from the upper surface and two measurements 1 mm. into the material from the lower surface. The figures presented in Table 2 are the average of the two fusion zone measurements.

In the series of measurements there was twenty readings of the parent metal hardness; these readings averaged 191 with a standard deviation of 3.4, implying a measurement accuracy and repeatability of about 2%.

Table 2. Welding Conditions, and Analysis of Welds

Weld#	78	77	79	75	76
Heat input (J/mm)	370	430	430	440	510
Laser Power (kW)	14	16	16	12	14
Welding speed(in/m)	88.4	88.4	87.2	64.6	64.6
Welding speed(cm/s)	3.74	3.74	3.69	2.73	2.73
Hardness measurements					
Near upper surface	247	256	234	228	226
Near lower surface	232	263	239	236	221
Ratio (Note 1)	1.06	0.97	0.98	0.97	0.98
Predictions from Adam's 2D Cooling time model and Yurioka hardness formulation.					
Time 800-500 (s)	10.5	14.2	14.2	14.9	20.0
Predicted hardness	257	236	236	234	221
Fusion zone Dimensions					
Upper width (mm)	2.45	1.85	2.6	2.22	2.65
Lower width (mm)	1.3	1.2	1.7	1.4	1.25
Energy of Fusion per unit length (J/mm)	38.5	31.3	44.2	37.2	40.1
Ratio of Energy of Fusion to Welding energy (%)	10.3	7.3	10.3	8.5	7.8
Signes variable H1 (note 2)	19.1	16.5	16.5	16.1	13.9
Signes variable H2 (note 2)	31.2	26.9	26.9	26.3	22.7

Note 1. Ratio is the ratio of the hardness near the upper surface to that near the lower surface.
Note 2. Units of H1 are inches cubed-degrees F/kJ. Units of H2 are that of H1 divided by square root of inches. See definitions in Section I.

Figure 4.

HARDNESS PROFILES OF LASER WELDS

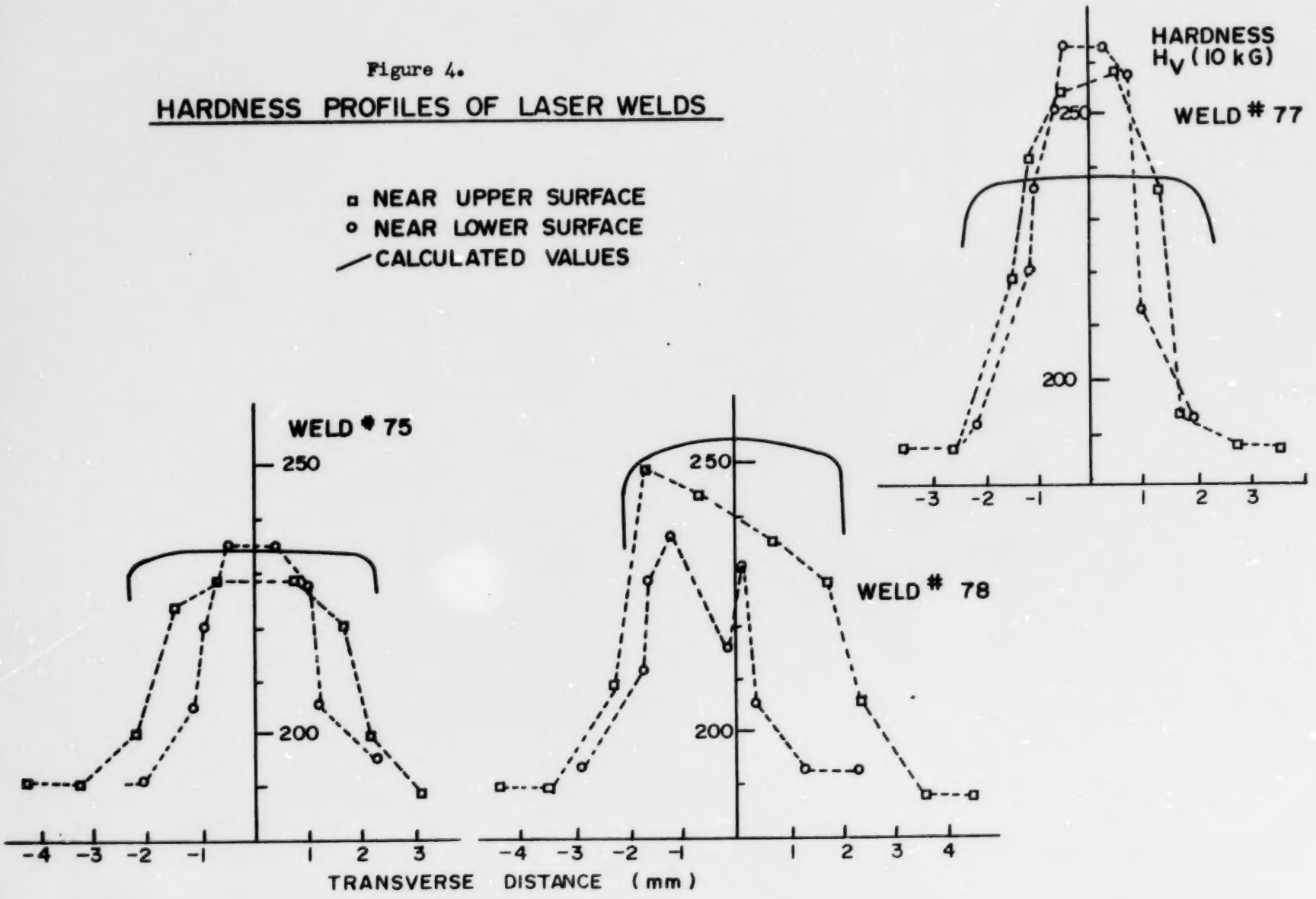

□ NEAR UPPER SURFACE
○ NEAR LOWER SURFACE
/ CALCULATED VALUES

Figure 5.

COMPARISON OF PREDICTED AND MEASURED HARDNESS OF LASER WELDS

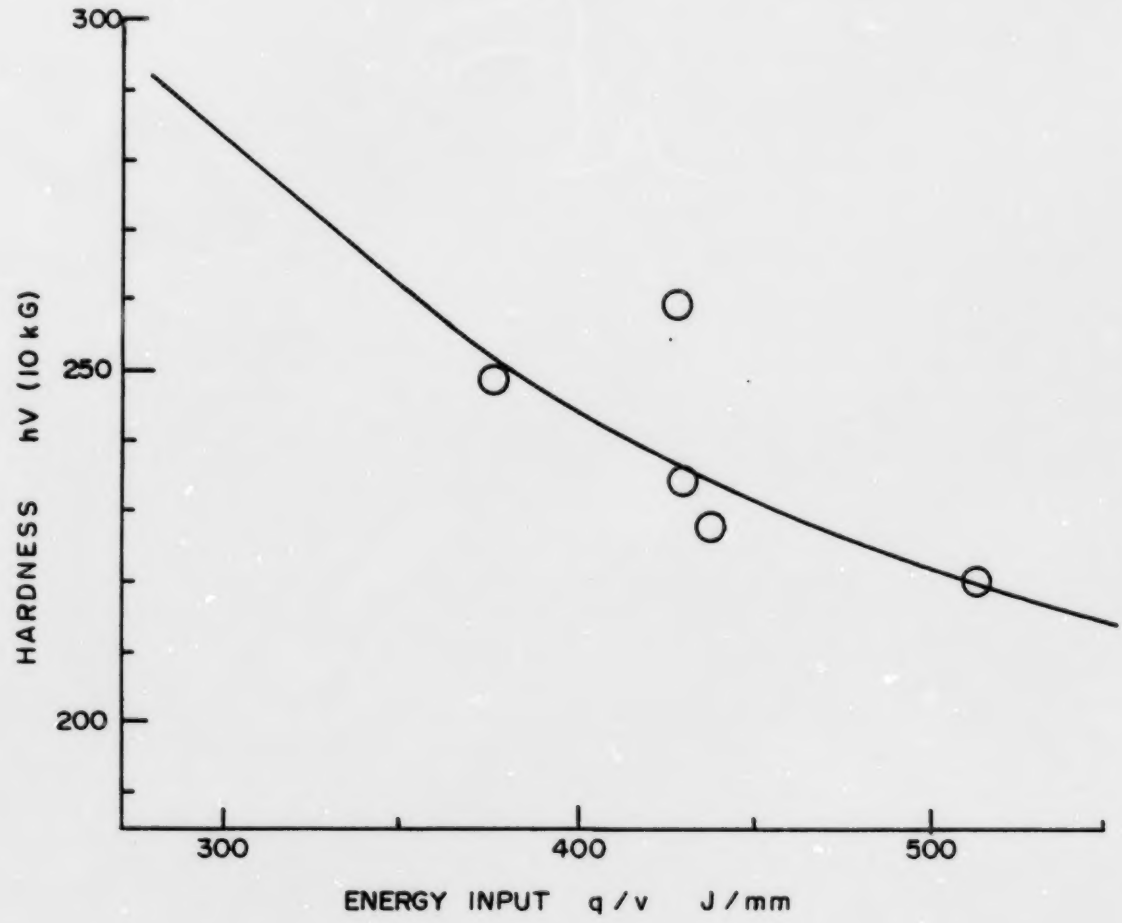

G. FUSION ZONE MEASUREMENTS

For the welds studies here, Table 2. shows the dimensions of the fusion zone. From a calculation of the cross sectional area, the energy needed to melt the metal once it has been heated to the melting point is calculated. The table also shows the ratio of this energy to the total energy needed to perform the weld. This ratio varies from 7.3 to 10.3%; in this small data set, there is no consistent dependence of this ratio on any other welding parameter.

A recent study (Metzbower, 1981) has compared the welding conditions and mechanical properties of welds in one half inch thick HY-130 steel made by different welding conditions. Table 3. summarizes the welding energy inputs, the volume of weld metal, and the fusion energy for different welding processes. It can be seen that for the deep penetration welding processes, the ratio of fusion energy to the total welding energy is at least twice that in the conventional welding processes.

Table 3.

Comparison of Fusion Energy in Various Welding Processes.

Welding Process	SMAW	GMAW	EB	LB
Number of Passes	7	5	1(note 1)	1
Energy input(kJ/cm)	79.8	58	4.45	7.2
Cross sectional area of fusion zone (sq.mm., see note 2)	128	123	27	29
Energy of fusion (kJ/cm)	2.8	2.6	0.59	0.62
Ratio energy of fusion to total energy input (%)	3.5	4.6	13.2	8.6

Note 1. The electron beam weld required two cosmetic passes in addition to the deep penetration pass. The energy of the cosmetic passes was not specified and is not included.

Note 2. Evaluated by this author from the cross sections presented in the above referenced paper.

Reference for Section G.

Metzbower, E.A., 1981. "Laser Welding", Naval Engineers Journal, pp. 49-58, August 1981.

H. Prediction of Hardness of Laser Welds and HAZs

After the keyhole has moved through the material, melting and vaporizing some of the metal, the temperature cools very rapidly because of the conduction of heat into the bulk of the material. The cooling rate (and the metal composition) determines the relative amounts of ferrite and pearlite and harder microstructures such as bainite and martensite, and thus the final hardness of the metal when cooled to room temperature. This is true for both the fusion zone and the heat affected zone in autogenous laser welding. Since no filler metal is used, the chemistry is assumed to be uniform through-out the cross section.

The 800C to 500C cooling time can be related to the resulting hardness of the material through a formulation devised by Yurioka and quoted in Shing, Bibby, and Goldak(1985). Yurioka's analytical expression takes into account the chemical composition of the steel and was a consequence of an experimental study of the cooling rates and resulting hardness in many types of steel. Amongst the steels studied were high yield strength line pipe with composition very similar to that used in the experimental program at Majestic Laser Systems (Yurioka, Ohsita, and Tamehiro, 1981).

The Yurioka formulation uses two carbon equivalents to relate the hardness to the 800C to 500C cooling time τ. These carbon equivalents are

$$CeqI = C + Si/24 + Mn/6 + Cu/15 + Ni/40 + Cr/6 + Mo/4 + (Nb+V)/5 + 10B.$$

$$CeqII = C - Si/30 + Mn/5 + Cu/5 + Ni/20 + Cr/4 + Mo/6 + 10B.$$

The resulting hardness is

$$H = 406*C + 164*CeqI + 183 - (369*C - 149*CeqI + 100)*Arctan(Y)$$

where

$$Y = (\log \tau - 2.822*CeqII + 0.262) / (0.526 - 0.195*CeqII).$$

The logarithm in the above equation is a common logarithm to base 10.

Figure 5 shows the hardness that would be predicted on evaluating the cooling rates by the Adams' 2D model which assumes that the heat is uniformly deposited through the cross section of the material as a line source. The Adam's 2D model is an analytical formulation that requires the assumption of a temperature independent value for the heat capacity of the material and the thermal conductivity of the material and implies the neglect of the specific heat of fusion and the heat of vaporization. The choice of values of the thermal constants used in the Adam's 2D formulation will be discussed later.

Figure 6 shows the dependence of temperature on time and on the distance away from the point of contact between the focussed laser beam and the steel surface. These curves were derived from the Adam's 2D formulation. As can be seen from the figure, as the distance between the point of observation and the point of contact increases, the peak temperature reached decreases and also the peak temperature occurs at successively later times. However the predicted 800-500C cooling time increases only very slightly as the distance from the point of contact increases, out to the point that the peak temperature does not reach 800C. Thus the predicted hardness throughout the weld metal and heat effected zone is approximately constant out to the point that the metal is not hardened at all. This is shown in Figure 4 which shows the predicted hardness distribution and compares with measured values. There is some scatter between the peak measured hardness and the peak predicted hardness which is also shown in Figure 5. In addition, in every case the measured distribution of hardness is significantly narrower than the predicted distribution.

References for Section H.

Shing, G.Y., Bibby, M.J., and Goldak, J.A. (1985). *A Microprocessor model for predicting the heat-affected-zone hardness of steel welds.* Soc. Amer. Manu. Prod. Eng. Quarterly, 16, #4.

Yurioka, N., Ohsita, S., and Tamehiro, H. (1981). *Study of carbon equivalents to access cold cracking tendency and hardness in steel welds*, presented at the Specialist Symposium on "Pipeline Welding in the 80's", Melbourne, Australia.

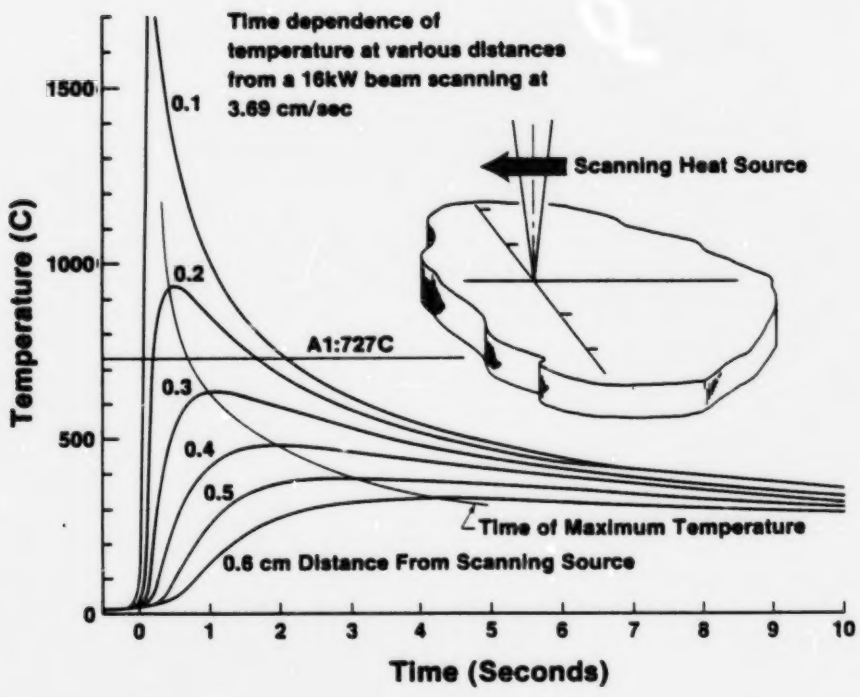

Figure 6. Dependence of temperature on time and distance away from scanning heat source.

I. Comments on prediction of Weld Cooling Rates.

Adam's 2D

Various approaches can be taken to estimating the cooling rate of the steel following laser welding. Adams(1958) has derived an analytical expression for the temperature distribution surrounding a line source moving through the material. The heat flow is reduced to a two dimensional problem. These circumstances are expected to most closely correspond to the heat flow away from a keyhole moving through the material when complete penetration is achieved in laser welding. The expression for the temperature distribution is

$$T(x,y) = To + \frac{q}{2\pi Kd} e^{m} K_o(\sqrt{m^2+n^2})$$

where $K_0(P)$ is the modified Bessel function of the second kind and zero order,.

d = material thickness
q = rate of heat input, in watts
K = thermal conductivity
m = $vx/2\alpha$
n = $vy/2\alpha$
v = relative velocity of source with respect to the plate
x = distance along welding direction (x=0 is position of source, x=vt is where source was time t ago.)
y = distance from the heat source path.
α = thermal diffusivity = $K/\rho C_p$.
ρ = density of plate
and C_p = specific heat of plate.

The Bessel function can be simplified for arguments greater than 2 or 3:

$$K_o(P) = e^{-P}\sqrt{\frac{\pi}{2P}}$$

With this approximation, the temperature becomes

$$T(x,y) = \frac{q \exp\left[m-\sqrt{m^2+n^2}\right]}{\sqrt{8\pi}\, Kp\, \left(m^2+n^2\right)^{1/4}}$$

The time dependence of the temperature evaluated at a fixed position on the welding axis (x=vt, y=0) depends on the welding parameters only through the heat input per unit length q/v. However when considering positions off the welding axis, then the heat input per unit time and the welding speed retain their importance individually. This is illustrated in Figure 7. which plots the cooling rates of welds calculated by the Adam's 2D model as the welding speed is varied over two orders of magnitude. It can be seen that for velocities greater than α/s, where α is the thermal

Figure 7.

COOLING RATES OF WELDS PERFORMED AT 525 J/mm (BY ADAM'S 2D MODEL)

A = 20 kW @ 3.81 cm/s

B = 2 kW @ 0.381 cm/s

C = 200 W @ 0.0381 cm/s

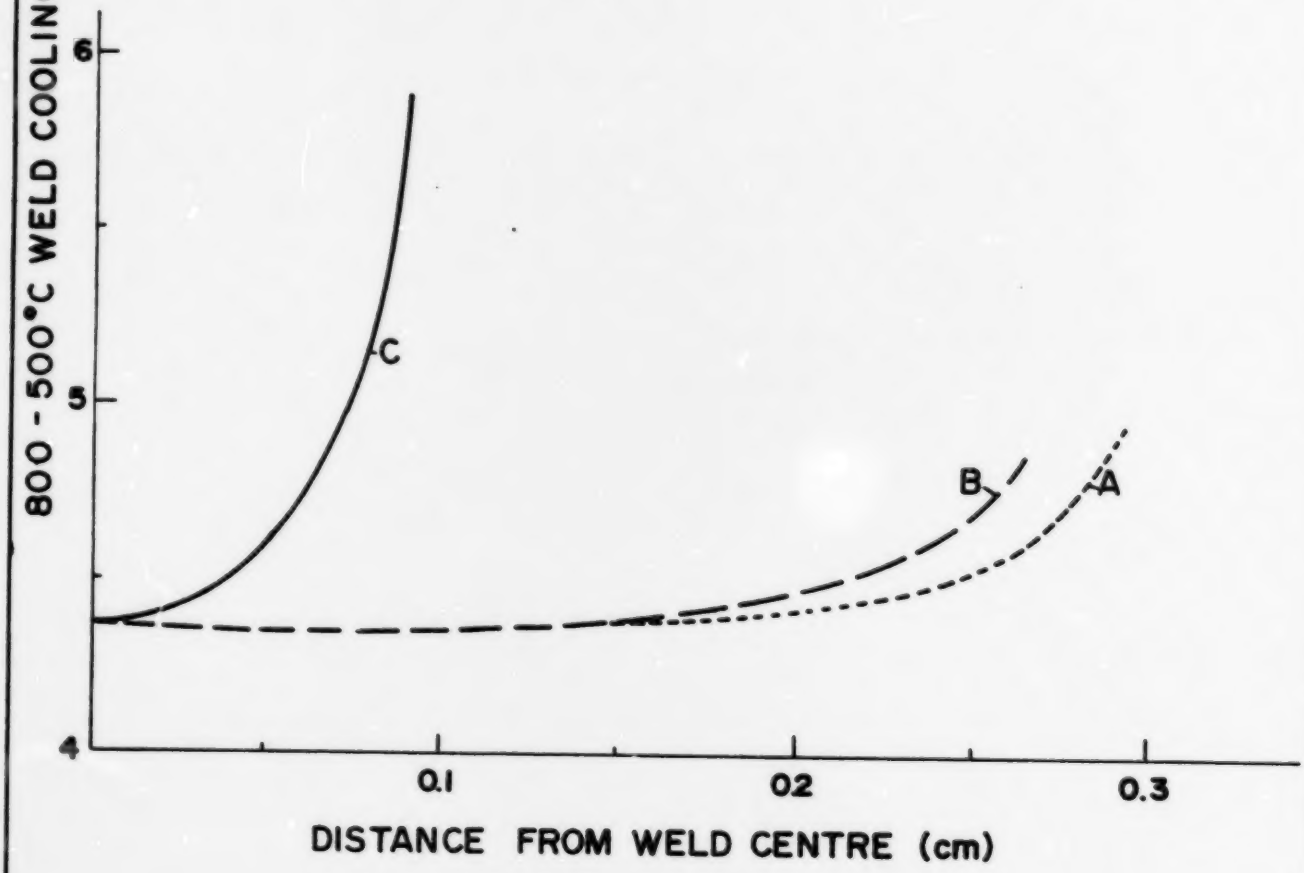

diffusivity and s is a typical distance, the cooling rate is independent of the distance from the weld center over a considerable range of distances. In this case one can use a cooling rate calculated for the weld centerline for the entire weld and heat affected zone. However for velocities less than α/s, a strong dependence on position is evident.

For speeds fast with respect to α/s, the heat flow is basically one dimensional. The heat is deposited on the weld centerline at high speed and flows perpendicularly away from the welding axis. At a particular position along the welding direction, by the time the heat has reached a point a couple of millimeters away from the axis, the heat source has moved a great distance away.

For slower speed, however, the heat flow becomes truly two dimensional, and heat flow in all directions (in the plane) away from the heat source is important.

On the welding axis (x=vt, y=0), the time it takes the metal at a particular position to cool from temperature T1 to a temperature T2 is calculated from the previous equation to be

$$t = \left(\frac{q/vd}{x_0}\right)^2 \qquad \text{(Eq'n I-1)}$$

where

$$x_0 = \left\{\frac{1}{4\pi K\rho C_p}\left[\frac{1}{(T_2 - T_0)^2} - \frac{1}{(T_1 - T_0)^2}\right]\right\}^{-1/2} \qquad \text{(Eq'n I-2)}$$

Adam's 3D

Adams has also derived an analytical expression for the case when the heat source moves not through the body of the material but over the surface of the material. In this case heat is conducted not only laterally away from the source, but also into the depth of the material which had not been directly heated by the source. This case, referred to here as the Adam's 3D case, had also been considered earlier by Rosenthal (1941).

Adam's 2.5D and 2D+R

A later paper (Jhaveri, Moffatt, and Adams, 1962) has considered the case where the heat source was a line source on one surface of the material. The material thickness assumed values such that the top and bottom surfaces of the plate have identical temperatures (the 2D case) or the thickness of the plate is so great that the temperature of the top plate is independent of the thickness (the 3D case). In between these two extremes is the 2.5D case where the thickness has a significant effect on the cooling rate. The authors also consider the possibility of substantial heat loss from the top surface of the material by radiation and convection. This is now called the 2D+R case. They quote an expression for cooling rates in this case in terms of the

surface coefficient of heat transfer. The various types of heat flow are summarized in Figure 8.

Signes' Work

Signes (1972) measured the cooling rates following gas metal arc, shielded metal arc, and submerged arc welding on plates of a variety of thicknesses, over a wide range of energy inputs. Signes defines two parameters H1 and H2 as follows:

$$H1 = p^{a}(1300 - T_o)/E \quad \text{and} \quad H2 = H1/\mathrm{sqrt}(p)$$

where T = preheat or base plate temperature, in degrees F,
p = thickness of the plate, in inches,
and E = Energy input in kiloJoules per inch.

A plot of cooling rate from the different welding processes versus the parameter H1 resulted in experimental guidelines for when the 2D case or 3D case is applicable, and for a correction factor to be used in the 2.5D case. This plot is shown as Figure 9. Here the vertical axis is proportional to the product of the measured cooling rate and the energy input per unit length. The horizontal axis is inversely proportional to the welding heat input but multiplied by the square of the thickness being considered. With these axis, the 2D case corresponds to those points which fall on a diagonal line through the origin. The slope of the diagonal line is $2\pi k\rho C_p$. Points representing welding conditions that result in 3D heat flow from a heat source moving over the surface of the material fall on a horizontal line. The vertical intercept of the horizontal line is $2\pi K$. The slope of the diagonal line through the origin and the intercept of horizontal line allow the determination of the effective thermal constants of the particular type of steel.

Between the region where the points clearly fall on the diagonal line and where the points fall on the horizontal line is a transition region. In this region the points appear to fall on a smooth curve that joins the diagonal and horizontal lines. This is the region where the 2.5D case is valid. Here the plate is not sufficiently thin that the top and bottom surfaces have the same temperature, in the Jhaveri *et al.* picture, or the heat source is not truly a line source of equal intensity at various depths.

This 2.5D case occurs for values of Signes' parameter H1 in the range of 8 to 20. The parameters H1 and H2 are evaluated in Table 2 for the laser welding conditions for which the hardness is considered here. The values of the parameter H1 fall into this range where the 2.5D case is pertinent. This implies that the keyhole created by the laser power does not represent a uniform heat source through the thickness of the workpiece. This had been expected since in some cases the observed cross sectional profile of the fusion zone was

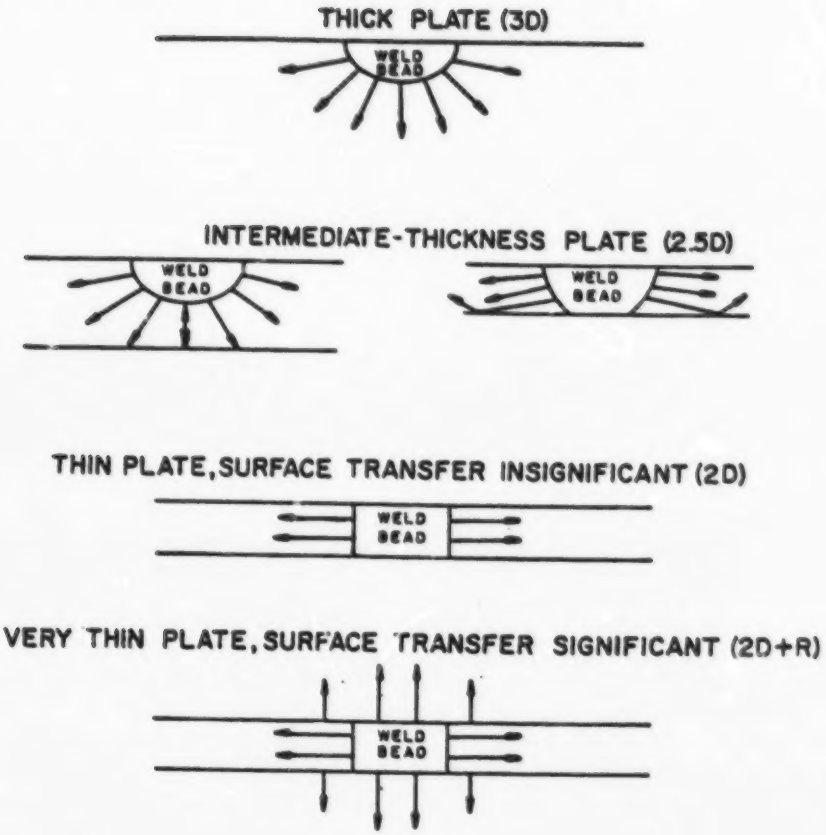

Figure 8. Four types of heat flow (from Signes(1972))

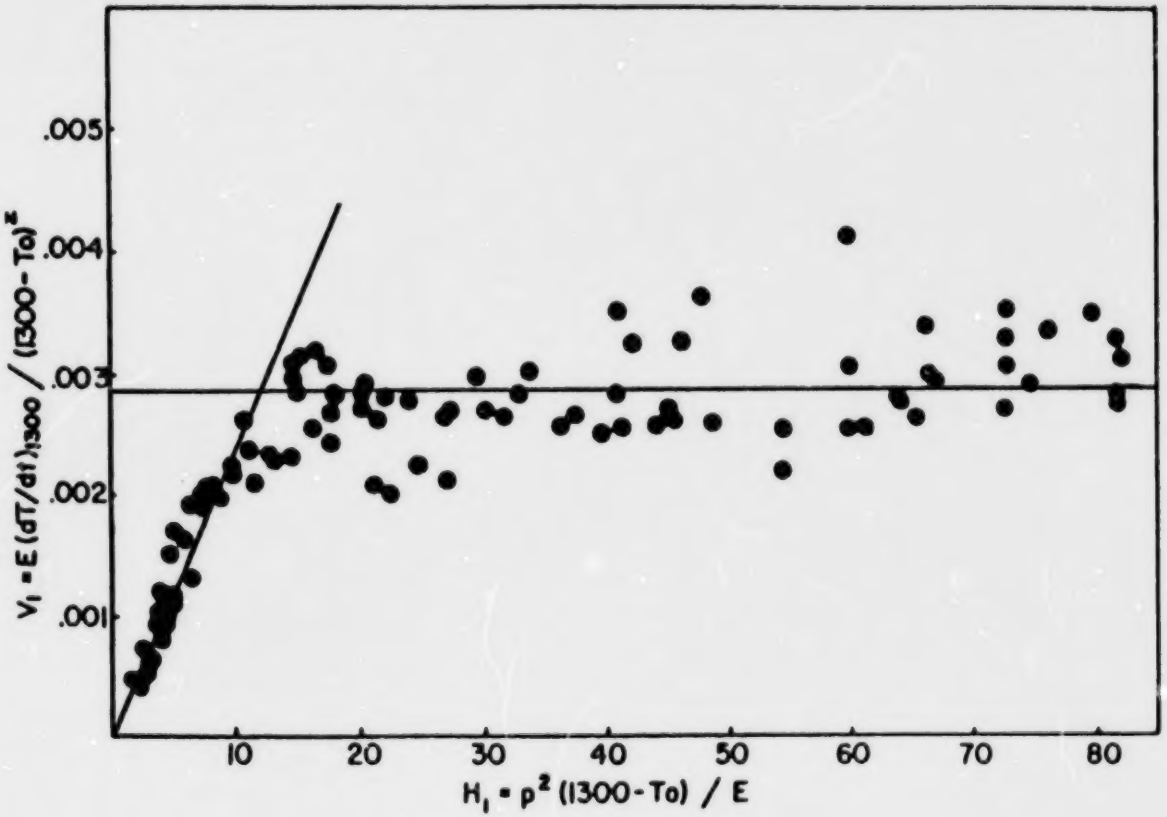

Figure 9. Signes' data for weld cooling rates.

trapezoidal, particularly when the penetration was marginally through the 9.5 mm. material thickness.

Signes plotted his data, obtained under a variety of welding conditions by a variety of methods, in a second graph that highlighted the cases where radiation and convection from the surface is important. For values of the parameter H2 less than 3.2 a correction has to be made to the Adam's 2D formula to account for surface losses. The application of the guidelines of Signes to the laser welding results presented here indicate that the radiative and convection losses are insignificant.

Boothby

Another relation between the cooling rate and the experimental conditions was derived by Cottrell and Bradstreet (1955). This was the result of measurements of the temperature following a SMAW arc by a thermocouple in the molton pool, in welds in plates over a range of thicknesses and preheat temperatures. This formulation was subsequently revised with results presented in Boothby (1985) to take into account later unpublished experimental work. The paper by Boothby also predicts the weld hardness from the cooling rates.

Comparison of different formulations

Fig. 10 is an indication of the comparative accuracy of the various cooling rate formulations, when applied to the welding conditions used here for laser welding. The curve indicated "Signes" corresponds to the Adams 2.5D case, as discussed above. With the exception of the Adams 3D model, which is inappropriate for these welding conditions, there is approximately a twenty-five percent variation between the various predictions of cooling rates. Here the Adam's 2D and 3D cases were calculated with values of the thermal constant's recommended by Shing, Bibby, and Goldak (1985), namely K=25 W/mC and C = 6E6 J/m3C. Values of the thermal constants found from Signes' work, and those used to fit the present experimental data in figures 4 and 5, were somewhat different.

There is some uncertainty involved in converting the cooling rate into the predicted hardness of the material. Various formulations, of which that due to Yurioka is only one, have been derived and are summarized by Shing, Bibby and Goldak (1985). These are based on experimental correlations between measured cooling rates and the consequent hardness in different types of steel. For a given cooling rate the predicted hardness by the different methods is somewhat different. However this is much less a source of inaccuracy than the actual calculations of the cooling rates.

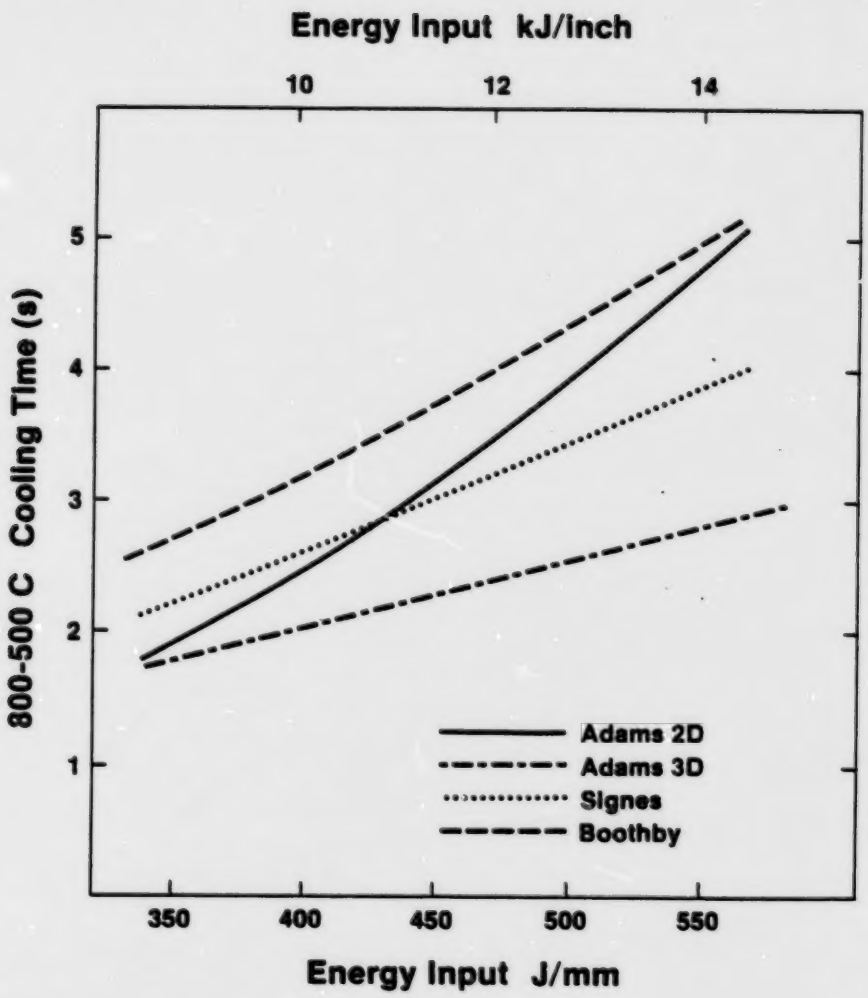

Figure 10. Comparison of different calculations of weld cooling rate.

Values of the Thermal Constants

Figures 11 and 12 show the temperature dependence of the specific heat and the thermal conductivity, respectively. Data from various sources is shown. The data from the Metals Handbook (American Society of Metals, 1961) is for pure iron only and is a tabulation of measured and calculated data. For the specific heat, measured values exist up to 1250 C only. Above this temperature, only calculated values of the specific heat are known. The figure also shows values of the specific heat of several steel alloys, from Smithell (Brandes, 1983). Where data is available, the temperature dependence seems to follow that of pure iron, although absolute values are somewhat lower. The absolute value decreases with increasing alloy content.

For the thermal conductivity, there are measured values up to 1300 C. Only two points are available in the liquid phase, and no data at all is available for the gas phase. Measurements for different steel alloys shown in figure 12 show the thermal conductivity drops sharply with increasing alloy content.

Other relevant data for pure iron is shown in Table 3. The data is from the Metals Handbook. Note that there is some uncertainty in the value of the boiling point of pure iron.

Table 3 Properties of Iron.

Density	7.87 gm/cm^3.
Melting Point	1530 C
Latent Heat of Fusion	65.5 cal/gm.
Boiling Point	3000 C
Latent Heat of Vaporization	1598 cal/gm.
A3: alpha to gamma phase transition	
temperature	910 C
latent heat	5.8 cal/gm.
A4: gamma to delta phase transition	
temperature	1390 C
latent heat	3.7 cal/gm.

Because both the thermal conductivity and the specific heat have a dramatic temperature dependence, it is difficult to characterize these metal properties by a single constant value. Nevertheless, this must be done if one is to make use of the simple analytical expressions such as those derived by Adams for the cooling rate following welding. As discussed above, plots of measured cooling rates against energy input can be used to determine effective values of the thermal parameters (Signes, 1972). However it has been shown that the effective thermal parameters have a significant dependence on the temperature at which the cooling rate is being measured (Graville, 1973) In particular, steels that undergo an austenite-to-ferrite transformation have different values of the thermal constants at temperatures exceeding the

Figure 11.

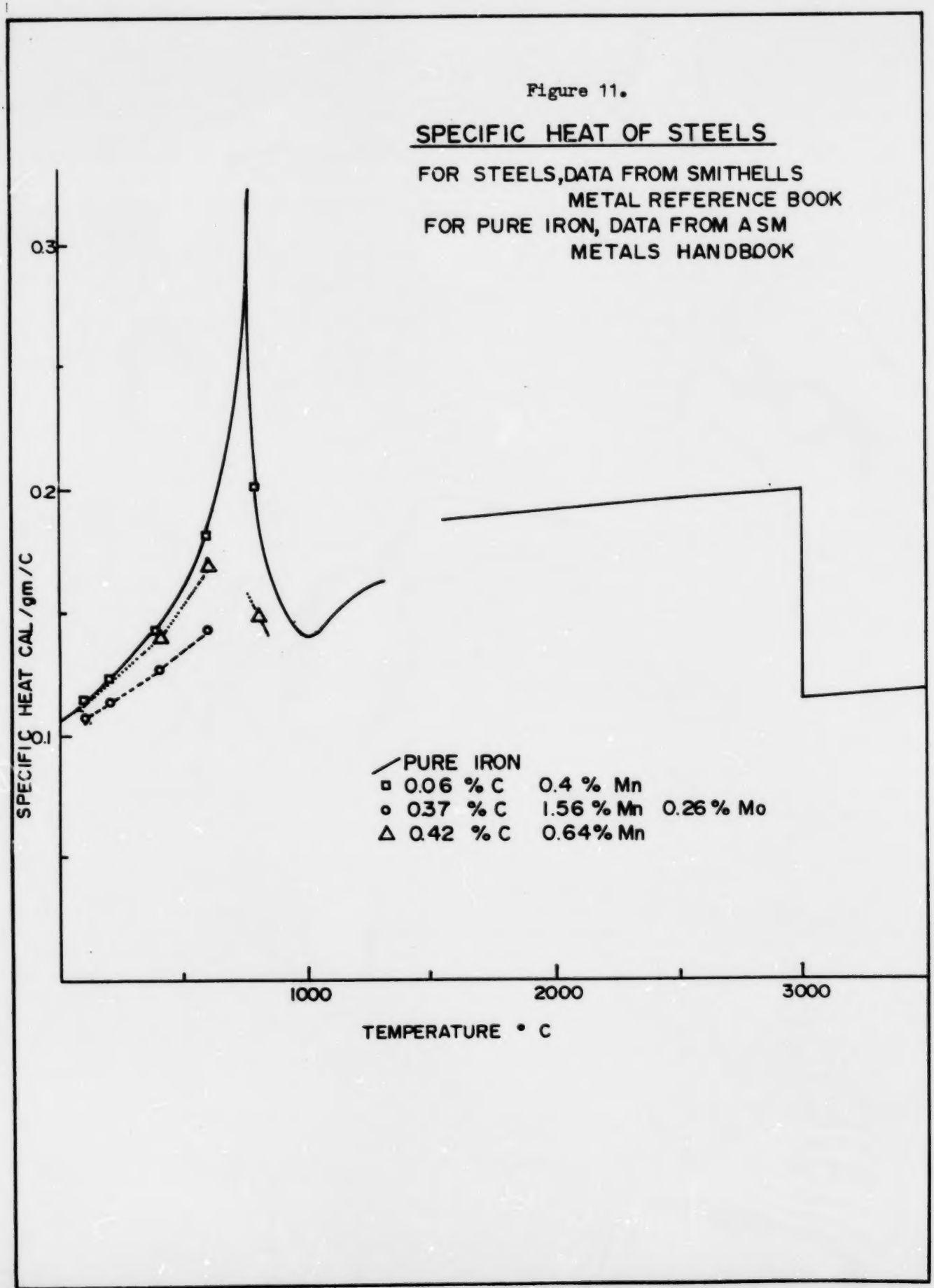
SPECIFIC HEAT OF STEELS
FOR STEELS, DATA FROM SMITHELLS METAL REFERENCE BOOK
FOR PURE IRON, DATA FROM ASM METALS HANDBOOK
SPECIFIC HEAT CAL/gm/C
0.3
0.2
0.1
PURE IRON
0.06 % C 0.4 % Mn
0.37 % C 1.56 % Mn 0.26 % Mo
0.42 % C 0.64% Mn
1000
2000
3000
TEMPERATURE • C

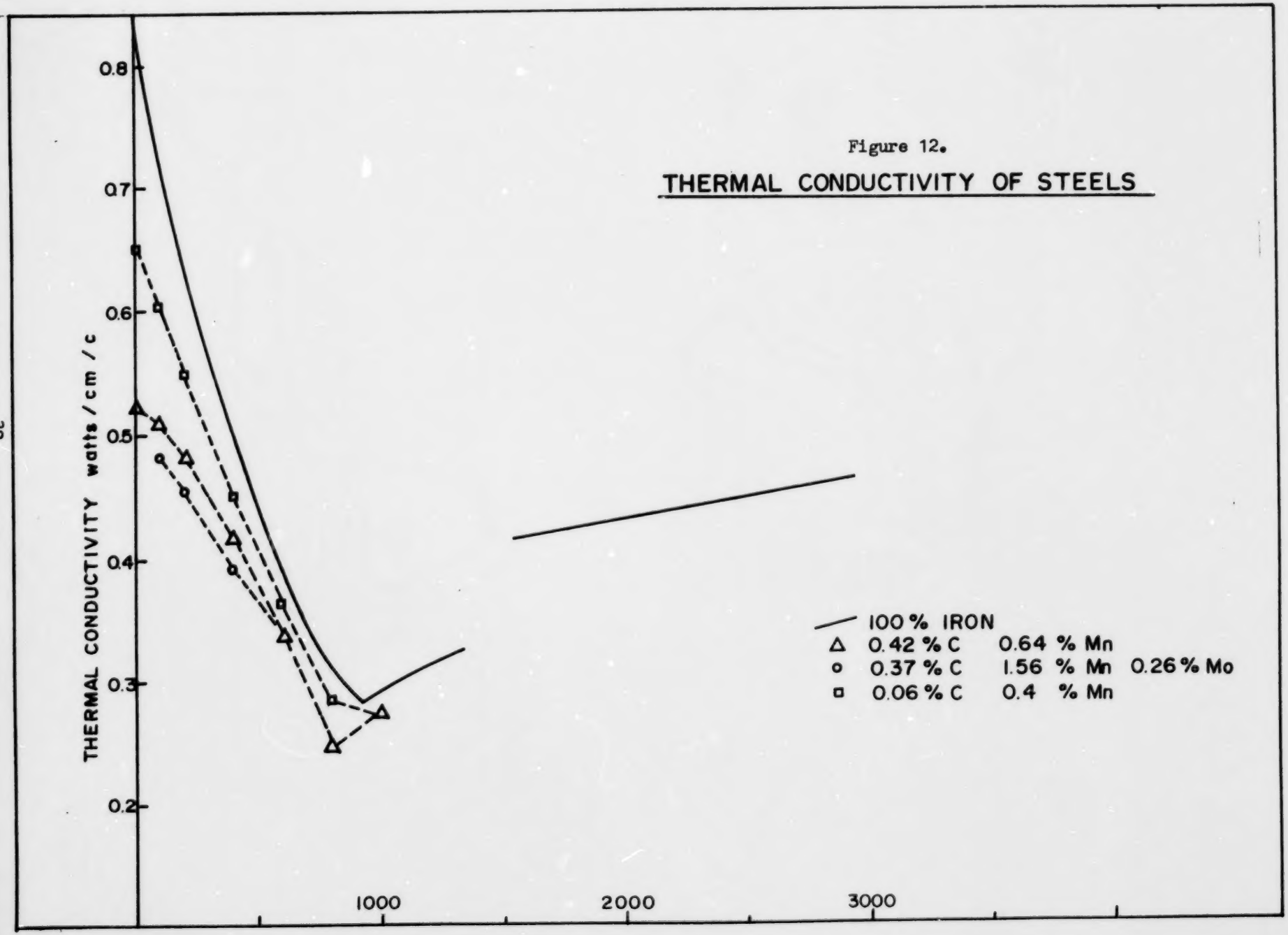

Figure 12.

THERMAL CONDUCTIVITY OF STEELS

transformation point from temperatures below the transformation point (Bibby, Eastman and Goldak, 1983).

One Dimensional Numerical Integration

In an attempt to show how serious the errors were in neglecting the explicit temperature dependence of the thermal constants, and in neglecting the latent heats of fusion and vaporization, a numerical integration which explicitly takes these factors into account was performed.

The numerical integration assumed a one dimensional heat flow, as shown in figure 13, but took into account the time dependence of the heat source. The numerical integration considered a one cm. long slice of material of 0.95 cm thickness, divided into twenty different plates or elements of width 0.05 cm. The heat source was incident onto slice #1, and the last slice was considered to be attached to a heat sink at room temperature. Heat was considered to flow both directions away from the slice on which it was deposited, but by symmetry it is only necessary to perform the calculations on one side.

For this calculation, the heat input at one element only was considered. The dependence of the heat input on time was assumed to be triangular; that is, it increased linearly in time reaching a peak after 0.5 seconds, then decreasing linearly in time so that no heat input occurred after 1.0 seconds. Heat flow from one element to the next in each 0.001 second interval, and the resulting temperature change of each element, were calculated. All the elements were initially assumed to be at room temperature. All time and space elements were the same, so this calculation cannot be considered to be at the same level of sophistication as Finite Element Calculations (Goldak, Patel, Bibby, and Moore, 1985).

For purposes of this numerical integration, the temperature dependence of the specific heat was assumed to be described by five straight lines, each line valid over a particular temperature range. This is an approximate alternative to a complete digitallation of the specific heat curve shown in figure 11, and using the digitallized data as input to the computer programme. Since, in any case, the specific heat for the particular alloy that was used for the welding studies is not known, the approximate technique used here is considered to be sufficiently accurate. A similar technique was used for the thermal conductivity; three straight lines each valid over a particular temperature range were used. The material density was considered to be a constant, independent of temperature; this implies that even if the material is vaporized, the metal vapor is trapped in the keyhole.

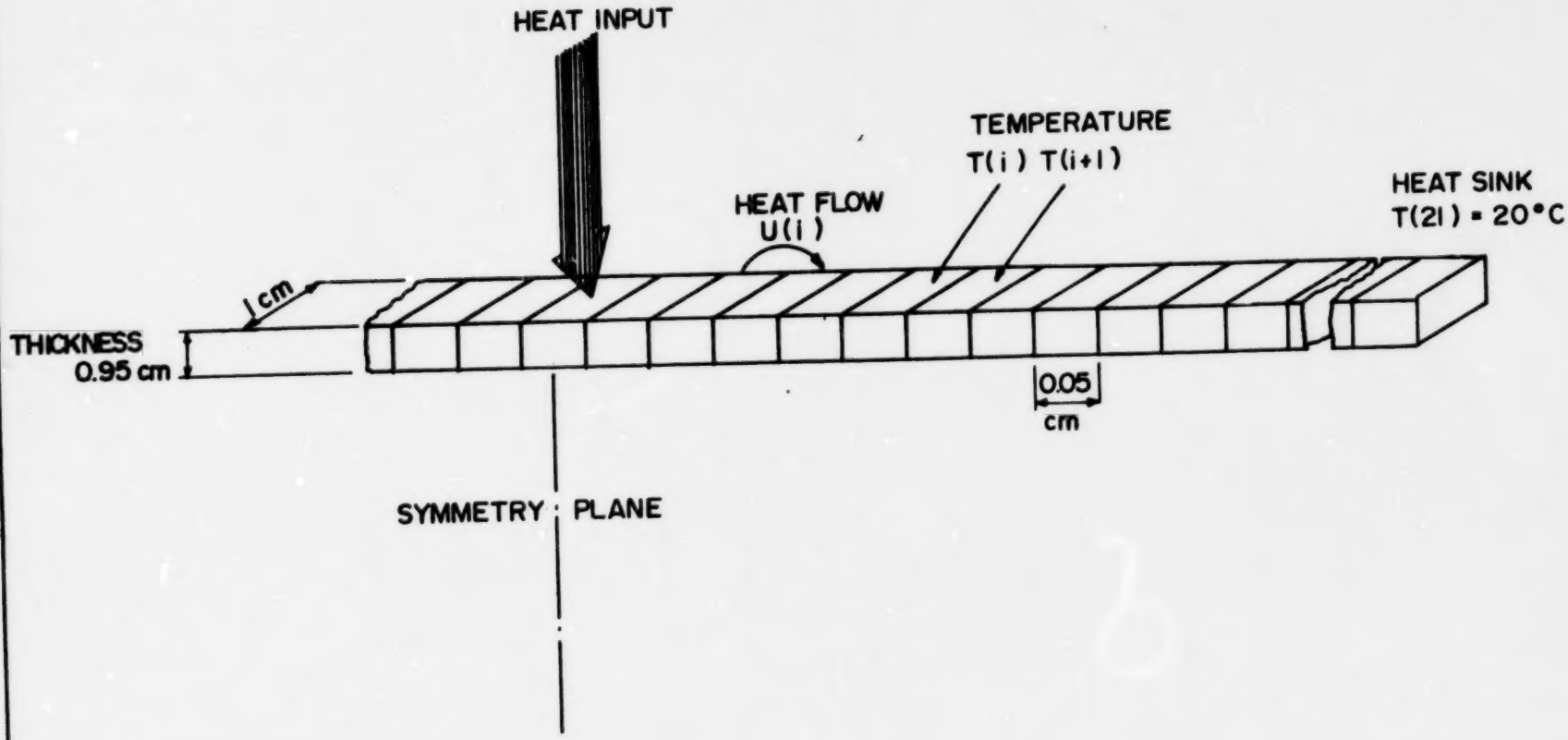

Figure 13.

GEOMETRY USED IN NUMERICAL CALCULATIONS

The calculations explicitly considered the effect of the latent heat of vaporization and fusion. However the latent heats associated with the metallurgical phase transitions were neglected.

Curve B in Figure 14 presents the results of the numerical integration, for one particular value of the laser power, for the temperature on the weld centerline. The temperature increases rapidly, hesitating momentarily at the melting point while the center element in the numerical integration gains the latent heat of fusion. Then the temperature increases again, reaching the boiling point. For the value of input power used here, the center element in the numerical integration never acquires the latent heat of vaporization required to vaporize the entire element. Thus only part of this element is vaporized and the temperature remains at the boiling point of steel. If in the computer program the latent heat of vaporization is put to zero, the temperature of this center element can continue to increase, as shown in curve C. The cooling time in the 800C to 500C range is not affected, however.

When the latent heat of fusion is put to zero, there is a large increase in the calculated weld centerline temperature as shown in curve D of figure 14. Moreover the width of the area in which the temperature exceeds the melting point increases from 0.1 cm for conditions corresponding to curve B (i.e. both latent heats are taken into account) to 1.2 cm for conditions corresponding to curve D (both latent heats put to zero). A molton pool of this dimension would certainly "drop out" and not be held in place by the surface tension forces. Thus it seems that calculations that neglect the latent heats cannot be expected to provide a good description of the welding process.

However, in spite of the fact that both the predicted peak temperature and the weld pool dimensions when neglecting the latent heats are much greater that when the latent heats are taken into account, the cooling rate is only different by 12%. The centerline cooling rate betwen 700 and 600C is 182C/s when latent heats are considered and 169C/s when they're neglected.

The numerical solution to the 1D heat flow problem was found when the data for the thermal conductivity in the liquid and gaseous states was increased by a factor of ten. The measured thermal conductivity presumeably refers to that in a stagnant pool of the liquid. However in the deep penetration welding process the liquid is in highly turbulent motion and heat transfer takes place as much by convection as it does by conduction. The increase in the data for the liquid thermal conductivity is intended to simulate the effect of the convective transfer. The results of the calculation, presented as curve A in figure 14, show that the enhanced

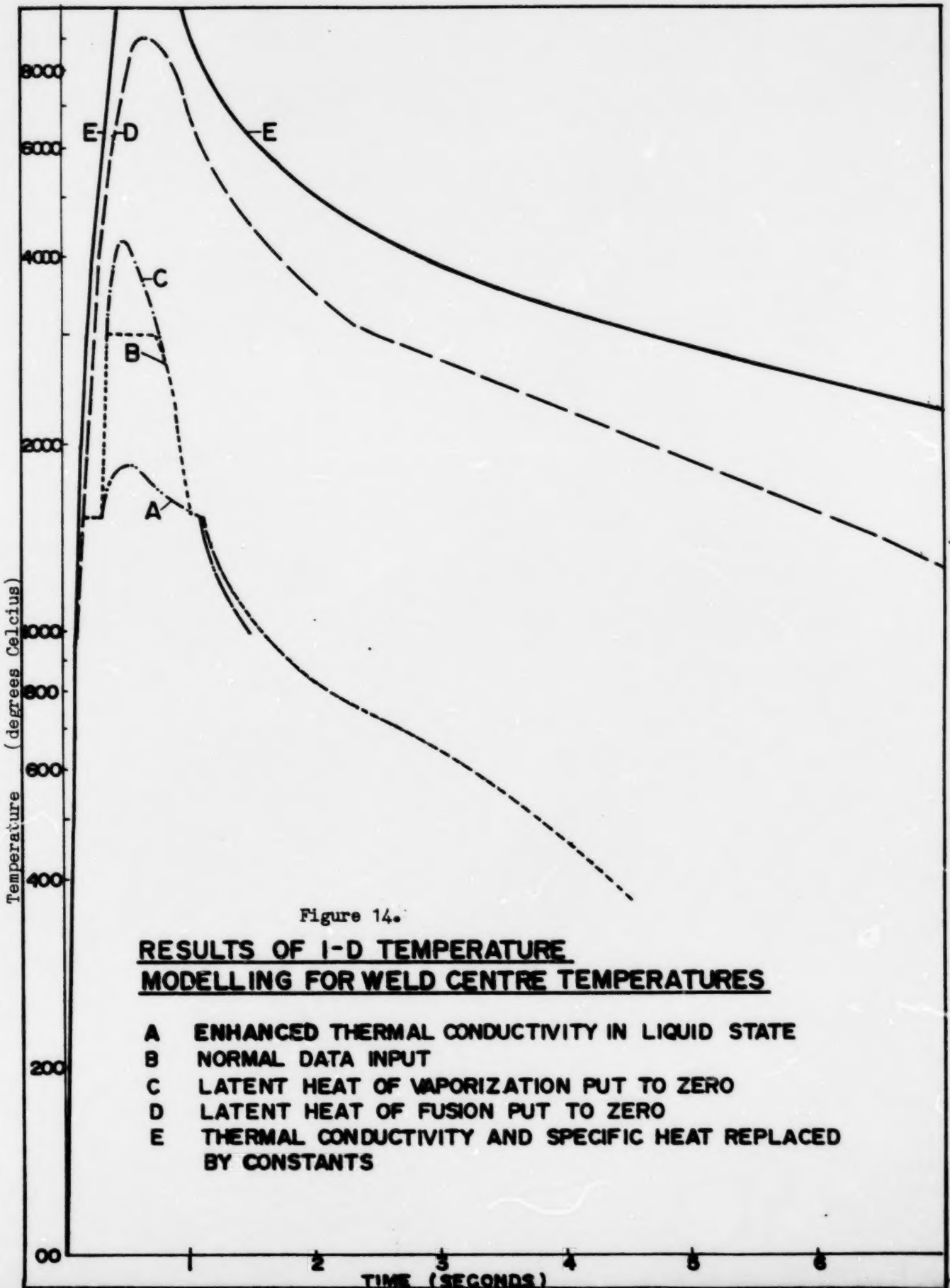

Figure 14.

RESULTS OF 1-D TEMPERATURE MODELLING FOR WELD CENTRE TEMPERATURES

A ENHANCED THERMAL CONDUCTIVITY IN LIQUID STATE
B NORMAL DATA INPUT
C LATENT HEAT OF VAPORIZATION PUT TO ZERO
D LATENT HEAT OF FUSION PUT TO ZERO
E THERMAL CONDUCTIVITY AND SPECIFIC HEAT REPLACED BY CONSTANTS

thermal losses in the liquid pool lower the peak temperature so that vaporization does not occur at these power levels.

The numerical calculation was also performed with the thermal conductivity and specific heat replaced by constant values. The values recommended by Shing, Bibby, and Goldak (1985) were used. The results of the calculation are shown by curve E on figure 14. The correctness of the result was confirmed by comparison with the results of an analytical solution of this one dimensional heat flow problem with a time varying heat input. The analytical solution could only be performed when constant thermal parameters are assumed, of course. The analytical and numerical solutions were identical. As mentioned above, the heat input was triangular in shape, reaching a peak after 0.5 seconds and with a duration of 1.0 seconds. The Adam's 2D solution, with the time origin shifted by 0.55 second, gave results which were indistinguishable from the two solutions of the 1D problem after the first second. (After 7 seconds the two solutions did differ slightly, with the Adam's 2D solution predicting somewhat higher temperatures and slower cooling rates. This was attributed to the fact that the Adam's solution considers an infinite workpiece whereas the computer solution considers a finite heat-sunk workpiece.)

However the cooling rates were significantly slower when constant thermal parameters were assumed than when thermal parameters with a realistic temperature variation were used as input in the computer calculations. By contrast, a recent comparison between the Adam's calculations and Finite Element Calculations had a 0.4% difference between cooling times when realistic temperature dependent thermal parameters instead of constant values were used (Moore, Bibby, Goldak, and Santyr, 1985). In this calculation larger differences were shown in the finite element calculations when a distributed source instead of a point source was used (1.6% difference), surface heat transfer was considered (14.4%), heat of transformation was considered (6.4%) and weld bead reinforcement was considered (3.2%). An unrealistic constant value for the thermal conductivity parameter seemed to compensate for the effects of neglecting the latent heats and bead reinforcement.

Thermal parameters for the Adam's 2D Model

Figure 5 shows the weld hardness data from the laser welds performed at Majestic Laser Systems. This figure also shows the hardness predicted from the Adam's 2D calculations in which the values of the thermal parameters had been varied to produce the best correspondance. The cooling time from 800C to 500C is evaluated using equations I-1 and I-2, and the hardness from the cooling time by the Yurioka formulation. From equation I-2 it is apparent that the cooling rate depends only on the product of the assumed values for the thermal conductivity and the heat capacity.

In plotting the spatial distribution of the cooling rates resulting from heating by a line source as in the Adam's 2D model, the width of the distribution is determined by the value chosen for the heat capacity, when the product of the thermal conductivity and heat capacity is assumed constant. The hardnesses shown as a function of position in figure 4 were calculated using the same value for heat capacity as that recommended by Shing *et al.* (1985).

However this was computed with different value of the thermal conductivity than that recommended by Shing *et al.* Both parameters differ from those calculated from the data in Signes' paper. This implies that the unrealistic constant value of the thermal parameters necessary to compensate for the effect of neglecting the latent heats is different in the case of the laser welding processes and in the conventional welding processes. Note that this result comes from taking welding conditions which are known to correspond to the 2.5D heat flow case, as discussed above, and attempting to fit the cooling rates to calculations based on a 2D model.

Published hardness data (Watson, 1985) from laser welds performed at The Welding Institute in two compositions of steel of 12.7 mm thickness is presented in figure 15. For completeness sake the hardness data from the Majestic Laser Systems welds are shown on the same figure, although steel of a different composition was used. Because the steels were different thicknesses, the hardness is plotted against the energy input per unit thickness. The solid lines in the figure show the predicted hardnesses for The Welding Institute steels. The hardnesses were predicted for three differents sets of thermal constants, as indicated by number in the figure. The thermal constants used are listed in Table 4.

The hardnesses predicted for the two Welding Institute steel compositions are almost identical, as shown in the figure for one value of the thermal constants. In this case agreement between the predicted values and the measured values required values for the thermal constants closer to those used with conventional welding processes (e.g. curve 2). For The Welding Institute welds, the speeds were considerable lower (0.3 to 1.2 m/min) and powers (5 to 8 kW) were considerably lower than those used in the Majestic Laser Systems' welds (1.6 to 2.2 m/min and 12 to 16 kW).

However the measured hardnesses for the two steels welded at The Welding Institute are significantly different. Here the primary difference in composition is that one steel was fully killed (0.46% Si, 0.023% Al) whereas the other steel was semi-killed (0.03% Si, 0.002% Al). The Yurioka formulation for predicting weld hardnesses from the cooling rate is obviously unable to respond to this compositional difference.

Figure 15.

MEASURED AND CALCULATED WELD HARDNESSES

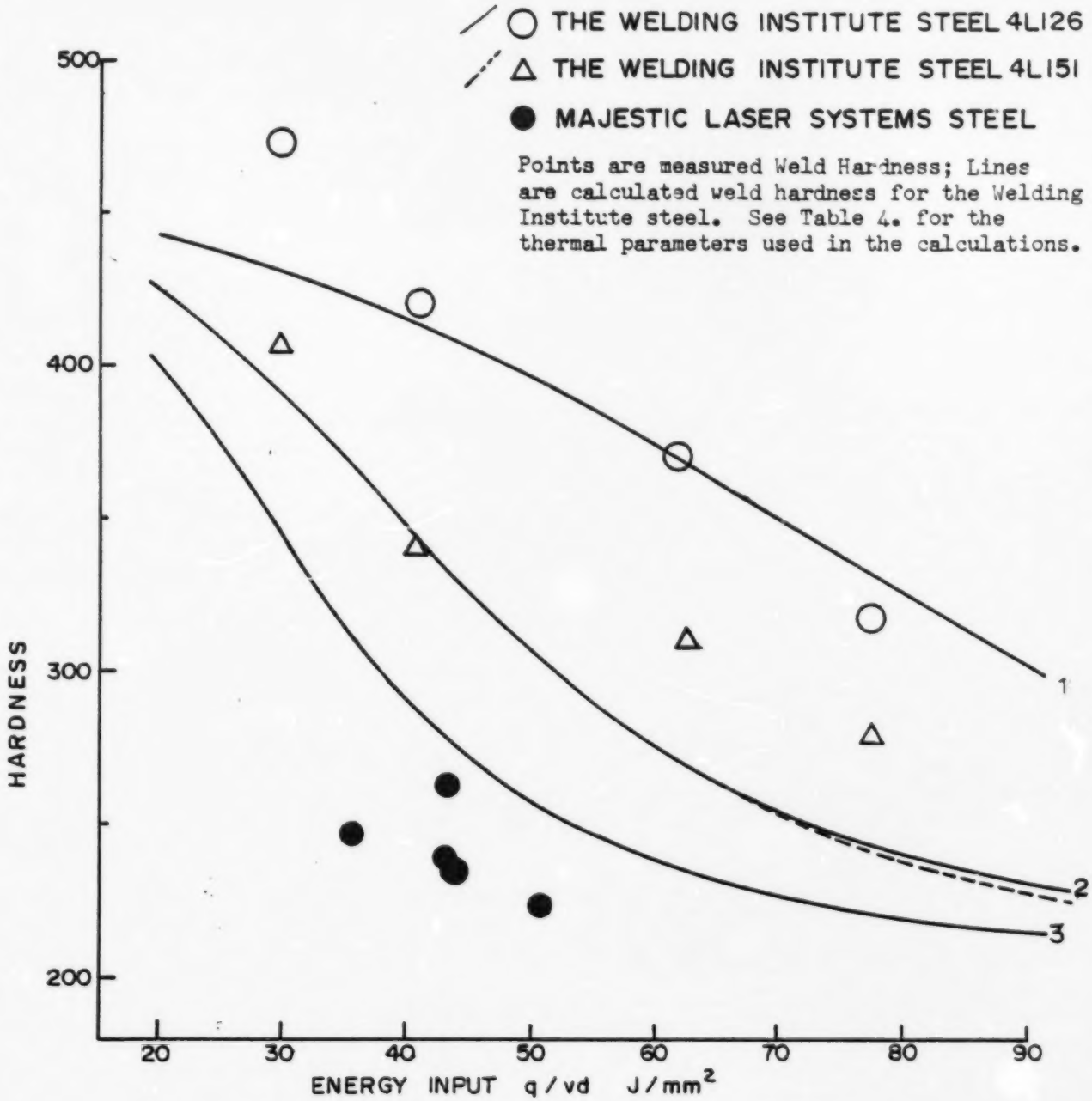

Table 4. Thermal Constants for the Adam's 2D Model

Curve	K	C	x	Source
1.	25	6E6	26.4	Shing *et al.*(1985)
2.	31.6	1.53E6	15.0	Calculated from Signes(1972)
3.	5.15	6E6	12	Best fit to present data
	W/mC	J/m3C	J/mm2	

References for Section I

Adams, Jr., C.M. (1958). *Cooling rates and Peak Temperatures in Fusion Welding.* Welding J.,37, no 5, 210s-215s.

American Society of Metals, 1961. Metals Handbook, Eighth Edition, Volume 1, Properties and Selection. Taylor Lyman, Editor. Published by the American Society of Metals, Metals Park, Ohio.

Bibby, M.J., Eastman, K., and Goldak, J.A., 1983. *The cooling behavior of deep penetration welds undergoing austenite-ferrite transformation*, Metallurgical Transactions B., Vol. 14B, 483-486.

Boothby, P.J. (1985). *Predicting hardness in steel HAZs.* Metal Construction, 17, no 6, 363-366.

Brandes, E.A., 1983. Smithells Metals Reference Book, Sixth Edition, E.A. Brandes, Editor. Butterworths, London.

Chemical Rubber Company, 1970. Handbook of Chemistry and Physics, 51st Edition, R.C. Weast, Editor. Published by the Chemical Rubber Company, Cleveland, Ohio.

Cottrell, C.L.M., and Bradstreet, B.J. (1955). *A method for calculating the effect of preheat on weldability.* Brit. Weld. J., 2, no 7, 305-309.

Duley, W.W., 1976. CO2 Lasers, Effects and Applications. Academic Press, New York.

Goldak, J., Patel, B., Bibby, M., and Moore, J., 1985. *Computational Weld Mechanics*, manuscript.

Graville, B.A., 1973. *Weld Cooling Rates and Heat-Affected Zone Hardnesss in a Carbon Steel,* Welding Journal, Research Supplement, vol.52, 377s-385s.

Jhaveri, P, Moffatt, W.G., and Adams, Jr., C.M. (1962) *The effect of plate thickness and radiation on heat flow in welding and cutting.* Welding J., 41, no 1, 12s-16s.

Rosenthal, D. (1941). *Mathematical theory of heat distribution during welding and cutting.* Welding Journal, 20, 220s-225s.

Shing, G.Y., Bibby, M.J., and Goldak, J.A. (1985). *A Microprocessor model for predicting the heat-affected-zone hardness of steel welds.* Soc. Amer. Manu. Prod. Eng. Quarterly, 16, #4.

Signes, E.G. (1972). *A simplified method for calculating cooling rates in mild and low alloy steel weld metals.* Welding Journal, 51, 473s-484s.

Watson, M.N. (1985). *Laser welding of 12.5mm thick niobium microalloyed structural steels at powers of up to 9kW.* Presented at the "2nd International Beam Technology Conference", Essen, W.Germany.

J. Special Features of Deep-Penetration Welding

From the Adams 2D temperature versus time and distance predictions mentioned above, the time duration for which the temperature at a given position exceeds the Austenization phase transition point can be evaluated. Results for the conditions corresponding to weld #77 in Table 2 are shown in Fig. 16. Hardening of the metal in the heat affected zone can occur only if the material is held above this phase transition temperature for a sufficiently long time that the carbon atoms can diffuse away from the carbide constituents and homogenize between the former carbide and ferrite constituents of the pearlite grain structure of the material. One can assume of course that if melting occurs complete homogenization occurs. If melting does not occur, this diffusion time is important. If insufficient time is allowed for the diffusion of carbon to result in a homogenous Austenitic structure, then the hardening cannot occur to the extent predicted by the weld cooling models. As can be seen from Fig. 16 only at the center portion of the weld, where melting occurs in any case, is the material kept above the A1 temperature for longer than a second. Thus the time-at-temperature may be a significant factor in the hardness distribution of laser welds. This occurs because of the high speed low energy input of the welds and makes this a much more important factor in laser welding than in other welding techniques.

(Note that figure 16 was calculated using values of the thermal constants recommended by Shing *et al*. The use of the values giving a best fit to the hardness values, as discussed in the previous section, results in a longer time exceeding the Austenization temperature.)

It was calculated in a previous section from the volume of metal in the fusion zone of laser welding that approximately 10% of the heat input is used as the latent heat of fusion. This latent heat energy is stored in the metal and is released late in the cooling cycle as the metal resolidifies. The results of the numerical integration of the heat flow equations show that the rate of resolidification is controlled by the rate at which the surrounding metal can conduct this heat away. Thus the release of this quantity of heat late in the cooling cycle distorts both the temporal and spatial dependence of temperature, as compared with the analytical formulations which neglect the latent heats of fusion and vaporization and assume constant values for the thermal parameters. This would be a more significant factor in deep penetration welding processes than in other processes, because the latent heat is a larger fraction of the total heat input in these cases.

The Adam's analytical models have had a reasonable success in predicting the weld cooling rates and other weld parameters. For example Christensen, Davies, and Gjermundsen(1964)

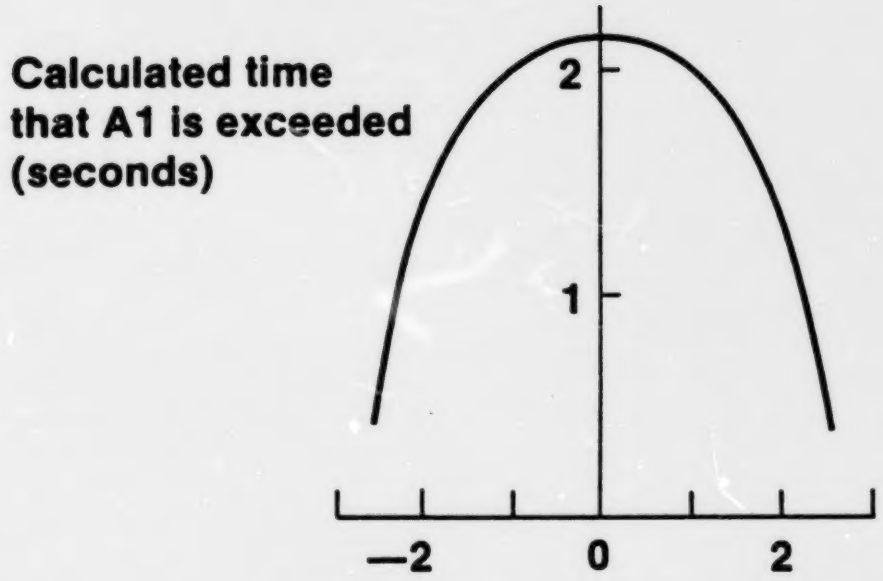

Figure 16.
Adam's 2D calculation of time that
A1 is exceeded in vicinity of weld centerline.
Transverse distance in millimeters.

calculated fusion zone dimensions produced by metal arc welding. It was pointed out in a previous section that this success was partially due to the use of unrealistic constant values for the thermal parameters, to compensate for the effect of neglecting the latent heats in the analytical models. In laser welding where latent heats are more significant than in conventional welding processes, different values of the thermal parameters must be chosen than those when using the same models for conventional welding processes.

Reference for Section J.

Christensen, N., Davies, V.de L., and Gjermundsen, K., 1965. *Distribution of Temperatures in Arc Welding*, Brit.Weld.J. 12, 54-75.